

Towards bridging the gap between motion capturing and biomechanical optimal control simulations

Tobias Gail*, Ramona Hoffmann[†], Markus Miezal[#], Gabriele Bleser[#], Sigrid Leyendecker*

[#] Department Computer Science
Technical University Kaiserslautern
Kaiserslautern, Germany
[miezal, bleser]@cs.uni-kl.de

* Chair of Applied Dynamics
University of Erlangen-Nuremberg
Erlangen, Germany
sigrid.leyendecker@ltd.uni-erlangen.de

[†] née Maas, Mathematical Methods in Dynamics and Durability
Fraunhofer Institute for Industrial Mathematics (ITWM)
Kaiserslautern, Germany
ramona.hoffmann@itwm.fraunhofer.de

ABSTRACT

Within this work, we make a first attempt towards improving human motion capture by combining motion capturing measurements and optimal control simulations of a human steering motion. We start with measurements obtained from a stationary optical system, a widespread capturing technology in biomechanics and movement science, under laboratory conditions. From an optimal control point of view, the goal is to increase the realism of simulated human motion through measurements. From a motion capturing point of view, the goal is to compensate for measurement sparsity, errors or lacks through meaningful assumptions based on biomechanical simulation. Our preliminary results show that a fusion of physical laws, biomechanical simulation and real data within an optimal control simulation framework indeed have the potential to improve motion capture and synthesis with respect to some of their inherent problems.

Keywords: optimal control simulation, optical motion capture, soft tissue artefacts, measurement sparsity.

1 INTRODUCTION

The abilities to capture and to simulate human motion are important enabling technologies for a wide range of applications in the professional as well as the private sector, ranging from health and ergonomics over human-machine-interaction to sports and games [15, 20, 4]. Different interdisciplinary research branches of computer science, mechanical engineering and mathematics are concerned with one or the other direction, i.e. with accurate and robust capturing or with realistic and physically plausible synthesis of human motion. Some of the most related disciplines include computer graphics, robotics and biomechanics. Though human motion capture and synthesis have been extensively studied and used, they are still subjects of research in the different domains. Moreover, this research often happens without bringing together the foundational knowledge, approaches and ideas that the different disciplines can offer.

There are methodically very different approaches to include optical measurement data in the simulation of human motion. Many are based on forward dynamics simulations, where ,e.g., the motion is constrained to follow the data followed by an inverse dynamics analysis to determine the corresponding control, see ,e.g., [5]. In [16], forward dynamic simulation is combined with an outer optimisation loop to find parameters producing a simulation that is most consistent with the data. Furthermore, a parametric control model is fitted to the data in [19], using the gains to identify the specific linear quadratic regulator cost function for a bicycle rider.

Within this work, we make a first attempt towards bridging this gap by investigating the specific scenario of combining motion capturing measurements of a human steering motion and optimal control simulations of this motion. While we aim at moving towards ambulatory motion capturing

systems in the long run, we start our investigation with a stationary optical systems, which is a widespread capturing technology in biomechanics and movement science. From a motion capturing point of view, the goal is to compensate for measurement errors or lacks and to reduce the required amount of measurements, while at the same time maintaining high precision, robustness and realism, all through meaningful assumptions based on biomechanical simulation. From an optimal control point of view, the goal is to resolve ambiguities and to personalise and increase the realism of simulated human motion guided through measurements.

1.1 Optical motion capture

Marker-based optical motion capture systems are typically based on a stationary infrastructure of high-resolution and high-speed infrared cameras, which are calibrated and synchronised with respect to each other. Retroreflective markers are then attached to specific human anatomical landmarks. These markers are tracked throughout the images of the multiple cameras and their trajectories are estimated in 3D space. Assuming some type of body model, most often a kinematic chain model [23], the motion of the subject is derived from the set of marker trajectories. Obviously, this requires (1) matching the dimensions of the digital model with the anthropometry of the human subject and (2) matching the digital marker positions with the real placement on the subject. The alignment is usually based on (functional) calibration, measurements and anthropometric tables, e.g., [17]. Available optical motion capture systems, e.g., from Vicon or NaturalPoint, are rather expensive, but widespread in biomechanics and ergonomics applications.

While the precision of measuring the marker positions can be extremely high, depending on the resolution and positioning of the cameras, there are a number of inherent problems and proposed solution paths: First, the sparsity of measurements in temporal and spatial domain and the risk of measurement lacks due to occlusions can be reduced by optimizing the camera placement and increasing the number of cameras, the camera update rate and the number of markers. However, this trades off with costs, setup time and wearing comfort. Second, deriving the underlying movement from the marker trajectories is usually based on the assumption that there is no relative motion between the external surface, where the markers are placed, and the modelled bone structure. Soft tissue artefacts, and further, simplifications of the body model and calibration errors, however, lead to violation of this assumption and can cause significant errors. A whole body of research tries to tackle this problem, e.g., based on new calibration procedures in combination with redundant marker sets (cluster markers) or more detailed biomechanical body models [9, 18, 6]. However, this often results in impractical setup procedures, e.g., a high number of markers to be positioned on the body or specific calibration infrastructure.

Instead of heavily relying on the measurements and trying to improve their quality, another promising approach is to embed more intelligence into the digital models, e.g., by including physics-based simulation, learnt motion models or higher-level knowledge about human motion [22, 7, 1]. The above approaches have already been used to improve optical motion capture, also based on monocular and multi-view markerless settings and when moving towards low-end and consumer systems.

1.2 Optimal control simulation

In general, an optimal control problem aims to find a trajectory of state and control variables, minimising an objective functional and fulfilling constraints in the form of differential equations as well as algebraic equalities and inequalities. The constraints represent the system's behaviour (e.g., its dynamics) as well as boundary conditions and path constraints, [8]. A solution to this mathematical model is approximated by a numerical simulation method [21, 3]. One problem of this abstract description is that the solution is found merely based on the technical model. When the problem is transformed (e.g., as in our approach) to a constrained optimisation problem, the optimising algorithm has no intuition on what is a natural and biologically realistic human motion. Human motion is controlled by the central nervous system taking into account an immensely

complex variety of aspects which are difficult to include in a mathematical description amenable to a simulation in acceptable time.

Another problem is the local nature of optimal control solutions (global optimisation is usually too demanding in terms of computational costs), thus the determined motion depends on an initial guess, which might be hard to find in the infinite number of possibilities to move from an initial to a final state. This is an obvious point where the combination with measurement data can be used to improve the efficiency and realism of human motion simulation. However, apart from the initial guess, the inclusion of data is possible in various parts of the optimal control problem formulation as is discussed in this work.

1.3 Our approach

We propose combining motion capture technology and optimal control simulations in order to tackle their inherent problems, i.e., compensate for measurement sparsity, lacks and errors, as well as shortcomings of digital body models and the curse-of-dimensionality related to the simulation space, while providing a realistic, natural and high-precision motion trajectory. We start with integrating measurements from a marker-based optical system into optimal control simulations based on a constrained optimisation framework [12]. In this first step, we investigate in particular the following aspects considering a human steering motion: (I) How should the measured marker positions be incorporated into the optimisation, i.e., in the objective function as so called soft constraints or as hard constraints to the optimisation? (II) When combining the measured marker positions with a physiologically motivated cost function, how far can the measurement update rate be reduced while still obtaining accurate, realistic and natural results?

In order to clarify these questions, we follow a systematic approach, performing a sequence of numerical experiments: First, we investigate (I) by considering only measured marker positions and the equations of motion. The result is then called *feasible solution*. Second, we combine the measured marker positions and the equations of motion with different established physiologically motivated terms in the cost function, in particular minimal torque and minimal torque change. These are then called *minimal torque solution* and *minimal torque change solution*. Third, we investigate (II) by gradually reducing the measurement update rate and looking at the resulting deviation of the simulated motion from the reference motion. For each solution, the reference motion is defined as the simulated motion, where all optical measurements are used (i.e. 100 Hz). The described deviation is used to assess the accuracy of the resulting motion. Moreover, realism and naturalness are assessed via the residual error with respect to the marker positions and the evolution of the joint torques.

The preliminary results show that a fusion of physical laws (i.e., the equations of motion), biomechanical simulation (i.e., physiologically motivated cost functions) and real data (i.e., optical marker positions) within an optimal control simulation framework indeed have the potential to improve motion capture and synthesis with respect to the above mentioned inherent problems.

2 MEASUREMENTS

Optical measurements are captured during different trials of a steering motion from one 30 year old male subject (height 176 cm) using the commercially available NaturalPoint OptiTrack system with twelve infrared cameras positioned on two heights around the steering wheel mockup. Two rigid bodies (with three retroreflective markers each) and six individual markers were attached to the subject's right shoulder, arm and hand: one rigid body on the shoulder and one on the back of the hand (above an inertial measurement unit, IMU), one marker on the upper arm, three around the elbow (close to lateral/medial epicondyl and elbow tip) and two on both sides of the wrist (close to ulnar and radial styloid processes). The markers were attached to a tight velcro jacket delivered with the system. After calibrating the optical system and measuring the dimensions of the subject and the positions of the markers with respect to the segments, steering motions were

| [meter] | mean | standard deviation |
|--------------------------|------|--------------------|
| Lateral/medial epicondyl | 0.09 | 3.4e-05 |
| elbow tip/ulnar styloid | 0.26 | 5.12e-04 |
| elbow tip/radial styloid | 0.28 | 5.73e-04 |
| ulnar/radial styloid | 0.10 | 5.58e-04 |

Table 1. Means and standard deviations in meters of pairwise marker distances with respect to markers on rigid segments. In an ideal world, the distances should be constant.

performed at different speeds while keeping the shoulder stationary. The 3D positions for the individual markers and the 3D positions and orientations for the two rigid bodies were captured at 100 Hz. Note that the hand’s rigid body position was corrected for the offset due to the IMU.

In the present study, only linear position information is used and the markers on the upper arm are also excluded, since the shoulder is assumed fixed. Hence, six marker positions are modelled (cf. Section 3). Moreover, for the experiments described in Section 4, a data sequence containing 50 sample points (0 to 0.49 seconds) showing a quarter turn with the right hand on the steering wheel mockup was extracted. Figure 1 shows the measurement setup. For future experiments, we also captured inertial measurements at 100 Hz from two IMUs attached to the upper and forearm. However, the data is not used in the present study. Note, when analysing the 3D marker positions



Figure 1. Measurement setup: stationary camera setup, attached markers and IMUs and start (middle) and end position (right) of the steering motion used in the experiments.

obtained from the optical system (e.g., by looking at the variations of pairwise marker distances on rigid segments), errors due to soft tissue artefacts can be noted (cf. Table 1), which motivates the investigation of this paper. Further observations regarding soft tissue artefacts are included in Section 4.

3 OPTIMAL CONTROL SIMULATION

3.1 Human arm model

For the simulation, the human arm is modelled as a multibody system consisting of three rigid bodies. A cylindrical upper arm is fixed in space by a spherical joint representing the shoulder. The elbow and wrist are modelled as cardan joints connecting the cylindrical forearm to the upper arm and the parallelepiped shaped hand to the forearm, respectively (cf. Figure 2). The bodies’ dimensions are personalised for the subject and the optical marker positions are placed manually in the model based on measurements as explained in Section 4.1. Thus, the exact definition of the personalised model is already a result from the measured data.

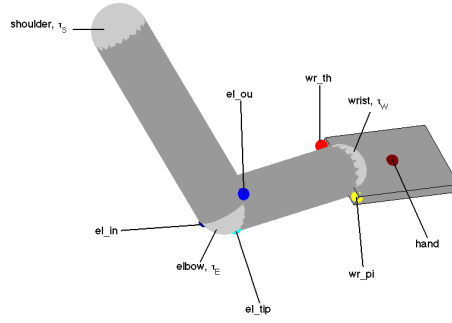


Figure 2. Human arm model with marker positions used for optimal control simulations. The three markers around the elbow are denoted el_in , el_out , el_tip . The two markers at the wrist are denoted wr_th and wr_pi . There is one marker on the hand.

3.2 Optimal control problem and simulation

Two inherently different approaches for the solution of an optimal control problem are the so called indirect (first optimise then discretise) and direct (first discretise then optimise) approach, see e.g., [21, 3]. In this work, a direct transcription method called discrete mechanics and optimal control for constrained systems (DMOCC), see [11, 14], falling into the latter class, is used to approximate the solution at the time nodes $t_0, t_1 = t_0 + h, \dots, t_N = t_0 + Nh$ on an equidistant time grid with time step h . As described in detail in [2], the kinematic description of the rigid multibody system is based on a redundant configuration variable $q_k \in \mathbb{R}^{36}, k = 0, \dots, N$ consisting of the placement of the centre of mass and the orientation represented by three directors that are aligned with the principal axes of inertia for each rigid body, respectively. A set of 29 holonomic constraints ensure orthonormality of each body's directors (thus they represent the columns of a rotation matrix) as well as the coupling by the joints, thus the complete model has 7 degrees of freedom. A nodal reparametrisation $F_d : \mathbb{R}^7 \rightarrow \mathbb{R}^{36}$ updates the redundant configuration $q_{k+1} = F_d(u_{k+1}, q_k)$ for $k = 0, \dots, N - 1$ in terms of discrete generalised coordinates $u_d = \{u_k\}_{k=1}^N$ with $u_k \in \mathbb{R}^7$ such that the constraints are fulfilled. In contrast to a formulation in terms of minimal coordinates (joint angles) from the beginning, this procedure ensures that rotations are always small and thus avoids the danger of singularities. The configuration variable q can be treated in a linear space, yielding a Lagrangian function with a constant mass matrix. A structure preserving scheme (symplectic-momentum with good energy behaviour) approximates the dynamics. It is derived via a discrete variational principle, see [13], where a discrete Lagrangian $L_d : \mathbb{R}^{29} \times \mathbb{R}^{29} \rightarrow \mathbb{R}$ approximates the action in one time interval. The discrete Euler-Lagrange equations resulting from the stationary condition for the discrete action are reduced to minimal dimension using a discrete null space matrix $P(q_k) \in \mathbb{R}^{29 \times 7}$ and the nodal reparametrisation F_d resulting in (2), see [2, 10]. They involve the left and right control forces $f_{k-1}^+ = B(q_k) \cdot \tau_{k-1}, f_k^- = B(q_k) \cdot \tau_k \in \mathbb{R}^{36}$ which are computed from the discrete generalised controls $\tau_d = \{\tau_k\}_{k=0}^{N-1}$ with joint torques $\tau_k \in \mathbb{R}^7$ (assumed to be constant during one time interval) using the input transformation matrix $B(q_k) \in \mathbb{R}^{7 \times 29}$, see [11] for a detailed introduction to DMOCC.

The optimal control problem is simulated solving the following nonlinear constrained optimisation problem using an SQP algorithm in Matlab. Minimisation of the objective function J_d

$$\min_{u_d, \tau_d} J_d(u_d, \tau_d) \quad (1)$$

subject to the fulfilment of the discrete equations of motion

$$P^T(q_k) \cdot [D_2 L_d(q_{k-1}, q_k) + D_1 L_d(q_k, F(u_{k+1}, q_k)) + f_{k-1}^+ + f_k^-] = 0 \quad (2)$$

boundary conditions

$$s(u_d, \tau_d) = 0 \quad (3)$$

and path constraints

$$h(u_d, \tau_d) \leq 0 \quad (4)$$

We perform optimal control simulations with different objective functions and path constraints. In order to address question (I), the measured marker positions are part of the objective function of the first problem in Section 3.2.1. This is sometimes called the inclusion of data as soft constraints and differs essentially from their appearance as hard constraints in Sections 3.2.2, 3.2.3 and 3.2.4, where the latter two involve commonly used physiologically motivated cost functions.

3.2.1 Minimisation of marker position residual errors

The goal of the first optimal control problem is to minimise the residual errors between the measured marker positions \bar{m}_k and the simulated marker positions m_k at all data points, thus the objective function

$$J_d(u_d, \tau_d) = \sum_{k=0}^N (m_k - \bar{m}_k)^T \cdot (m_k - \bar{m}_k)$$

is minimised subject to the discrete equations of motion (2) and boundary conditions (3), while no further path constraints are present.

3.2.2 Feasible trajectory

State and control trajectories that are feasible in the sense that they fulfil the equations of motion (2) and boundary conditions (3) are obtained by minimising the objective

$$J_d(u_d, \tau_d) = 1$$

with the additional path constraints (4) imposing an upper bound $\varepsilon \in \mathbb{R}$ on the marker position's residual errors taking the form

$$h(u_d, \tau_d) = \sum_{k=0}^N (m_k - \bar{m}_k)^T \cdot (m_k - \bar{m}_k) - \varepsilon \quad (5)$$

3.2.3 Minimisation of torque

The third problem minimises the control effort

$$J_d(u_d, \tau_d) = \frac{\Delta t}{2} \sum_{k=0}^{N-1} \tau_k^T \cdot \tau_k$$

subject to the discrete equations of motion (2), boundary conditions (3) and path constraints (5).

3.2.4 Minimisation of torque change

In the last problem, the temporal torque change is minimised, thus

$$J_d(u_d, \tau_d) = \frac{\Delta t}{2} \sum_{k=0}^{N-2} \left\| \frac{\tau_{k+1} - \tau_k}{\Delta t} \right\|^2$$

while the discrete equations of motion (2), boundary conditions (3) and path constraints (5) are fulfilled.

4 RESULTS

Simulation experiments are carried out based on the extracted data sequence as described in Section 2 with the different optimal control problems introduced in Section 3. Here, we first make some remarks concerning optimal control simulation (and its initialisation) with regard to aspect (I) mentioned in Section 1. Then, observations on the soft tissue artefacts are discussed. Finally, addressing (II), we present results from simulations based on gradually reducing the measurement update rate of the recorded data.

4.1 Simulation of the optimal control problem

As mentioned in Section 3.1, the personalised model results from the measurements, more precisely from the measurement \bar{m}_0 at the first pose at $t_0 = 0$. Geometrical data like lengths and radii of the rigid bodies, placement of joints and joint axes as well as the marker placement on the segments and their initial configuration (placement and orientation) are obtained from \bar{m}_0 via a geometric and inverse kinematic analysis. All numerical experiments start in this pose at rest, which is the only boundary condition (3). Note that no end point condition is formulated since the motion did neither end at rest nor at a known velocity and for a measurement rate of 100 Hz in combination with the chosen time grid with a time step of $h = 0.01$ s and $N = 49$, thus 50 measurements $\bar{m}_0, \dots, \bar{m}_N$, the number of measurements and simulated configurations coincides such that the residual error at the final point $m_N - \bar{m}_N$ controls the final configuration. Based on the obtained geometrical data, for all experiments, the initial guess for the optimisation parameters u_d is obtained from the measured marker positions $\bar{m}_k, k = 1, \dots, N$ via inverse kinematics. The initial guess for the joint torque trajectory τ_d is zero everywhere.

First, the state and control trajectories minimising the marker position residual errors described in Section 3.2.1 are approximated. The resulting configuration trajectory fits the measured data up to a residual error of $\varepsilon = 0.0218$, which is used as the upper bound in the inequality path constraints (5) of the following experiments. The largest residual errors occur around the elbow towards the end of the motion. While in the later experiments, the torque evolutions are qualitatively and quantitatively similar in large parts of the motion, see Figures 7, 8 and 9, the torque evolution in this experiment is more jerky and assumes absolute values that are up to 1.75 times larger. Using the number of SQP iterations required by the optimiser until convergence as an indicator for efficiency, this experiment is by far the most inefficient, requiring approximately 20 times more iterations than the feasible solution and approximately 10 times more than the torque minimising and torque change minimising simulations.

For the feasible, torque minimising and torque change minimising simulations described in Sections 3.2.2, 3.2.3 and 3.2.4, the initial guess is determined as described above when all measurements, i.e., a measurement rate of 100 Hz, are used. However, when reducing the measurement update rate, only every n^{th} measurement with $n \in \{2, \dots, 13\}$ is taken into account in Equation (5) and ε is reduced accordingly. Consequently, the poses determined by inverse kinematics from the measurements $\bar{m}_{nk}, k = 1, \dots, N \text{div} n$ are used either as a piecewise constant initial guess or the configuration q is interpolated linearly. Note that the last measured data point which is included in all reduced rate experiments is \bar{m}_{39} .

For the three objective functions (feasible, minimising torque and minimising torque change), the two initial guess strategies (piecewise constant and piecewise linear) and the 13 measurement rates (every n^{th} measurement with $n \in \{1, \dots, 13\}$), a total of 78 optimal control simulations is evaluated in the sequel.

4.2 Soft tissue artefacts

In addition to the soft tissue artefacts discussed in Section 2 that can be observed directly in the measurement data (cf. Table 1), when investigating the residual errors with respect to the marker positions for the three numerical experiments (full measurement rate) in Figure 3, most dominant errors are visible for the three markers around the elbow, with an additional trend of accumulating error from the start to the end of the motion. This can be explained by soft tissue artefacts during the turning motion, where the velcro jacket, to which the markers are attached, slightly slides over the skin. When being solely based on measurements (i.e., ignoring physics-based and biomechanical constraints), such artefacts would result in an erroneous motion, in this case underestimating the amount of turning.

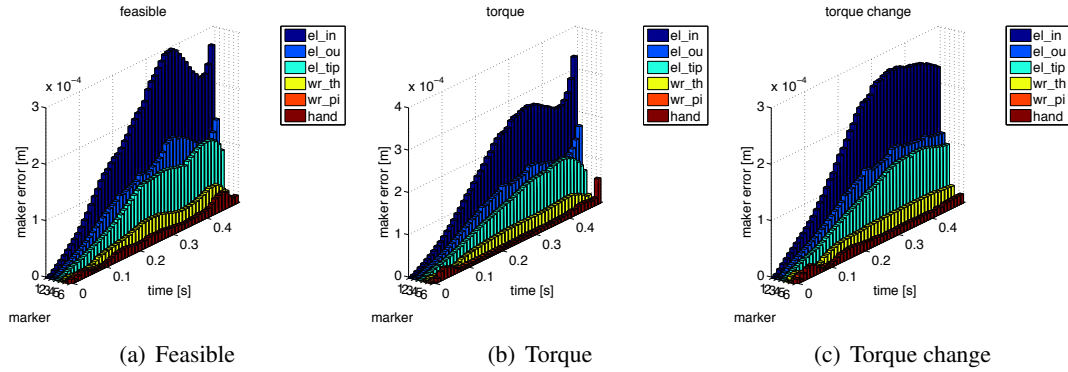


Figure 3. Residual errors with respect to marker positions (distance between simulated and measured marker position for each sample point) at 100 Hz measurement rate.

4.3 Simulations with reduced measurement rate

Reducing the measurement update rate as explained in Section 4.1 results in a range between 100 and 7.69 Hz. Figures 4 and 5 show the error statistics for the tested measurement rates based on a piecewise constant and a piecewise linear initial guess, respectively. Error is here defined as the Euclidean distance between the configurations q obtained from the reference simulation (using a measurement frequency of 100 Hz in the feasible, torque minimising and torque change minimising simulation) and the simulation with reduced measurement update rate at each time node $t_k, k = 0, \dots, N$. The figures then report the average error and its standard deviation for a complete simulation (y-axis) over the measurement rate (x-axis). Each vertical line (illustrating the standard deviation) represents one successful simulation. Missing vertical lines indicate a simulation failure, e.g., due to divergence of the SQP algorithm. Note that errors are computed only in the time interval $[0, 0.39]$ s, since \bar{m}_{39} is the last measurement used in all simulations. When comparing Figures 4 and 5, in particular the close-ups, it can be observed that some simulation experiments have failed below 20 Hz when using a piecewise constant initialisation. Hence, linear interpolation enables convergence at very low measurement update rates. Moreover, it can be seen in the figures that linear interpolation also reduces the overall errors. This is particularly visible for the feasible solution.

When looking at Figure 5, as expected, the errors and standard deviations increase with reduced measurement update rate for all solutions. However, the error of the feasible solution is consistently higher than the error of the solutions including a physiological cost function term. Below 20

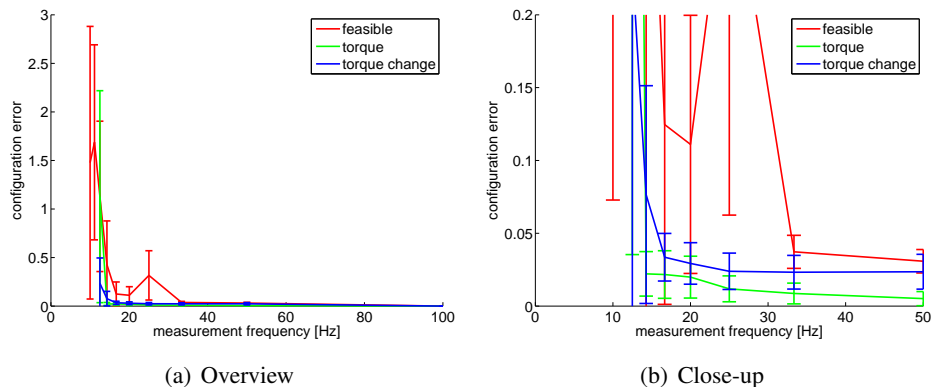


Figure 4. Mean errors and standard deviations based on piecewise constant initial guess.

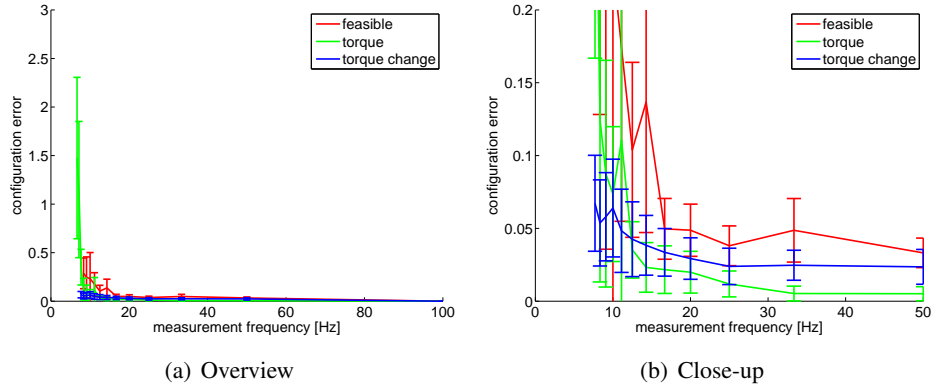


Figure 5. Mean errors and standard deviations based on piecewise linear interpolation for initial guess.

Hz, errors and standard deviations of the feasible solution increase significantly and the last two simulations even fail. In contrast, minimising torque and torque change show a better behaviour. Minimal torque shows the lowest error until 12.5 Hz, however, then starts to increase significantly, and fails for the last simulation at 7.69 Hz. Minimal torque change successfully converges for all experiments and shows a comparably small error increase even at the lowest measurement frequencies. These observations confirm that, in our experimental settings, biomechanical simulation can compensate for low measurement update rates. Moreover, while the torque minimising solution provides the most accurate results down to a certain measurement rate, the torque change minimising solution provides acceptable accuracy for even lower measurement update rates, hence adds further stability. To provide more detailed insights, Figure 6 illustrates the error evolution in q (configuration error) for two concrete measurement update rates (using linear interpolation for the initial guess). We chose 33.3 Hz (every 3rd measurement) as representative for a mid-range frequency and 8.33 Hz (every 12th measurement) as lowest frequency with results for all solutions.

These figures confirm the above observations. In addition, it is nicely visible in Figure 6(b), that the errors show a periodic pattern induced by the measurement update rate, i.e., the error becomes lower around measurement points. This is most apparent for the feasible solution, but also clearly visible for the minimal torque solution. Interestingly, the minimal torque change solution, even if showing a slightly higher error than the minimal torque solution for the mid-range frequency, is much less affected by the measurement points. This might indicate a higher independence from measurements, a better ability to deal with errors in these and, as a result, a higher robustness. On the other hand, also error of the time stepping equations (with respect to an analytical solution) grows as the simulation advances in time. This point needs further investigation in the future. One

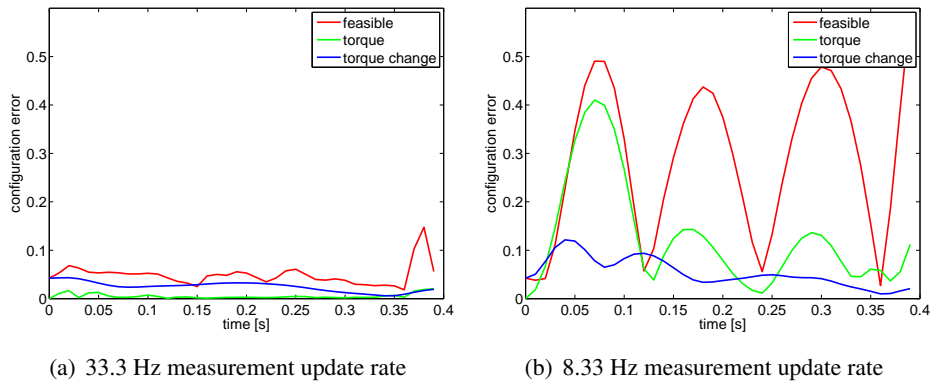


Figure 6. Error evolution in configuration q .

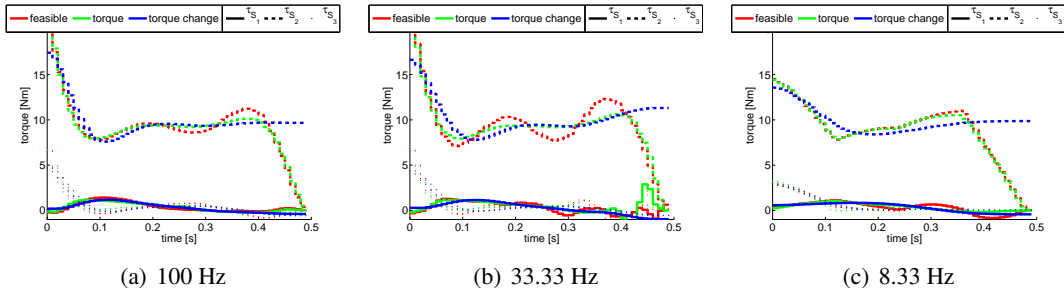


Figure 7. Estimated torques in the shoulder.

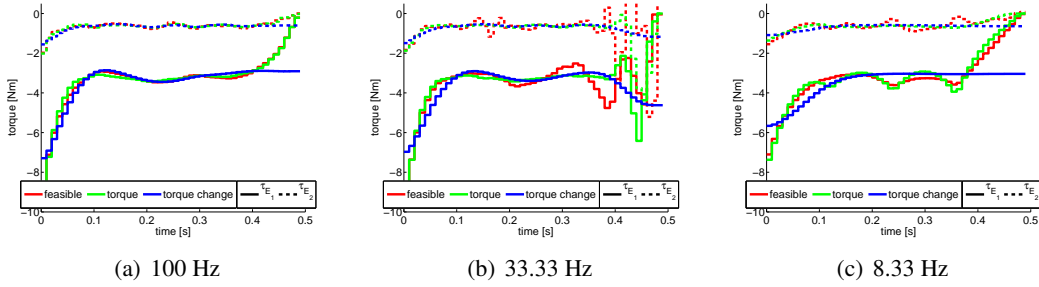


Figure 8. Estimated torques in the elbow.

can also observe that the error tends to decrease throughout the simulation, in particular for the low measurement update rate and the minimal torque and torque change solutions.

Moreover, the evolutions of the joint torques in shoulder, elbow and wrist are shown for the three numerical experiments in Figures 7, 8 and 9, respectively. Note that only the torque evolution in the time interval $[0, 0.39]$ s can be compared, since \bar{m}_{39} is the last measurement used in all simulations. Two observations can be made here: First, when decreasing the frequency from 100 to 8.33 Hz, the resulting torques of the feasible and minimal torque solution change more significantly than the minimal torque change solution. This is most visible for the wrist. Second, with reduced measurement update rate, the feasible and minimal torque solutions show jerky torque changes, though the actual motion is smooth. Again, this is most apparent for the wrist. In contrast, the minimal torque change solution shows smooth torque changes. This is not surprising, since minimal torque change is an optimisation criterion. However, even when not having ground truth torque at hand, together with the first observation, the smooth torque evolution seems more consistent and plausible, being the origin of a natural motion. Hence, the minimal torque change solution seems to provide torques, which are less dependent on measurements and which indicate a more natural human motion, which are both wanted effects of our study.

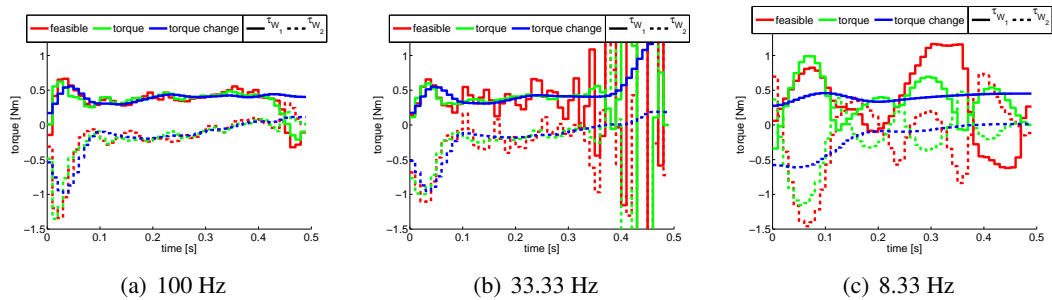


Figure 9. Estimated torques in the wrist.

5 CONCLUSIONS

Since the inclusion of the measurements as soft constraints by minimising the residual errors in the objective function turns out to be way more inefficient than their inclusion as hard constraints, the purpose of the first numerical experiment is mainly to determine the bound ε for the later experiments. Also considering that the measurements are a priori known to have errors indicates that it is more promising to use them as guiding points and to define an environment around them where a solution of a biomechanical simulation with a physiologically motivated objective is to be found. From the investigated objective functions here, minimising torque change shows the most realistic and natural results and the highest stability with respect to the reduction of the measurement frequency.

The most obvious future task is to confirm these observations with different types of motions and other physiologically motivated objective functions. Furthermore, it is worthwhile to take into account also measurements of the bodies orientation instead of only marker point positions and information on the accelerations and angular velocities measured from inertial sensors. In particular, the latter means not merely the inclusion of more and different type of data, but the move towards ambulatory motion capturing may overcome many of the shortcomings of optical stationary systems discussed in the introduction and enable a wide range of applications outside the lab. However, also many technical aspects need to be investigated. If there is knowledge on the precession or error-proneness of certain measurements, weighting factors can be introduced accordingly. Secondly, not only the measurement rate, but also the number of marker positions can be reduced, excluding ,e.g., those with most soft tissue artefacts.

Finally, the inclusion of further information known about the considered motion, like the presence of obstacles in the environment or contact to the surroundings, as ,e.g., of the hand moving on a circle due to its contact to the steering wheel, may help to increase the realism and naturalness of the simulated motion.

REFERENCES

- [1] I. Akhter and M. J. Black. Pose-conditioned joint angle limits for 3D human pose reconstruction. In *IEEE Conf. on Computer Vision and Pattern Recognition (CVPR) 2015*, June 2015.
- [2] P. Betsch and S. Leyendecker. The discrete null space method for the energy consistent integration of constrained mechanical systems. Part II: Multibody dynamics. *Int. J. Numer. Meth. Engng.*, 67(4):499–552, 2006.
- [3] J. Betts. Survey of numerical methods for trajectory optimization. *Journal of Guidance, Control, and Dynamics*, 21(2):193–207, 1998.
- [4] G. Bleser, D. Steffen, A. Reiss, M. Weber, G. Hendeby, and L. Fradet. *Smart Health - Open Problems and Future Challenges*, volume 8700 of *Lecture Notes in Computer Science (LNCS)*, chapter Personalized Physical Activity Monitoring Using Wearable Sensors, pages 99–124. Springer, 2015.
- [5] J. Cooper and D. Ballard. Realtime, physics-based marker following. *Motion in Games. Lecture Notes in Computer Science*, 7660:350–361, 2012.
- [6] H. De Rosario, Á. Page, A. Besa, and Á. Valera. Propagation of soft tissue artifacts to the center of rotation: A model for the correction of functional calibration techniques. *Journal of Biomechanics*, 46(15):2619–2625, 2013.
- [7] D. J. Fleet. Motion models for people tracking. In *Visual Analysis of Humans*, pages 171–198. Springer, 2011.

- [8] M. Hinze, R. Pinnau, M. Ulbrich, and S. Ulbrich. *Optimization with PDE constraints*. Springer, Berlin, 2009.
- [9] S. H. Lee. *Biomechanical modeling and control of the human body for computer animation*. ProQuest, 2008.
- [10] S. Leyendecker, J. Marsden, and M. Ortiz. Variational integrators for constrained dynamical systems. *ZAMM*, 88(9):677–708, 2008.
- [11] S. Leyendecker, S. Ober-Blöbaum, J. Marsden, and M. Ortiz. Discrete mechanics and optimal control for constrained systems. *Optimal Control Applications & Methods*, 31(6):505–528, 2010. DOI: 10.1002/oca.912.
- [12] R. Maas and S. Leyendecker. Biomechanical optimal control of human arm motion. *Journal of Multi-body Dynamics*, 2013. DOI 10.1177/1464419313488363.
- [13] J. Marsden and M. West. Discrete mechanics and variational integrators. *Acta Numerica*, 10:357–514, 2001.
- [14] S. Ober-Blöbaum, O. Junge, and J. Marsden. Discrete mechanics and optimal control: an analysis. *ESAIM: Control Optimisation and Calculus of Variations*, 17(2):322–352, 2010. DOI: 10.1051/cocv/2010012.
- [15] S. Patel, H. Park, P. Bonato, L. Chan, and M. Rodgers. A review of wearable sensors and systems with application in rehabilitation. *J Neuroeng Rehabil*, 9:21, 2012.
- [16] C. Remy and D. Thelen. Optimal estimation of dynamically consistent kinematics and kinetics for forward dynamic simulation of gait. *Journal of biomechanical engineering*, 131(3), 2009. doi:10.1115/1.3005148.
- [17] O. Rettig, L. Fradet, P. Kasten, P. Raiss, and S. I. Wolf. A new kinematic model of the upper extremity based on functional joint parameter determination for shoulder and elbow. *Gait & posture*, 30(4):469–476, 2009.
- [18] T. Ryu. Application of soft tissue artifact compensation using displacement dependency between anatomical landmarks and skin markers. *Anatomy Research International*, 2012.
- [19] A. Schwab, P. de Lange, and J. Moore. Rider optimal control identification in bicycling. In *Proceedings of the ASME 2012, 5th Annual Dynamic Systems and Control Conference*, pages 201–206, , 2012. doi:10.1115/DSCC2012-MOVIC2012-8587.
- [20] N. Vignais, M. Miezal, G. Bleser, K. Mura, D. Gorecky, and F. Marin. Innovative system for real-time ergonomic feedback in industrial manufacturing. *Applied Ergonomics*, 44(4):566 – 574, 2013.
- [21] O. von Stryk and R. Bulirsch. Direct and indirect methods for trajectory optimization. *Annals of Operations Research*, pages 357–373, 1992.
- [22] M. Vondrak, L. Sigal, and O. C. Jenkins. Dynamical simulation priors for human motion tracking. *Pattern Analysis and Machine Intelligence, IEEE Transactions on*, 35(1):52–65, 2013.
- [23] V. M. Zatsiorsky. *Kinematics of human motion*. Human Kinetics, 1998.